Title
Comparison of electric field enhancements: linear and triangular oligomers versus hexagonal arrays of plasmonic nanospheres.

Journal
Optics express, 21(7)

ISSN
1094-4087

Authors
Campione, Salvatore
Adams, Sarah M
Ragan, Regina
et al.

Publication Date
2013-04-08

Comparison of electric field enhancements: Linear and triangular oligomers versus hexagonal arrays of plasmonic nanospheres

Salvatore Campione,[1] Sarah M. Adams,[2] Regina Ragan,[2] and Filippo Capolino[1,*]

[1]*Department of Electrical Engineering and Computer Science, University of California, Irvine, CA, 92697, USA*
[2]*Department of Chemical Engineering and Materials Science, University of California, Irvine, CA, 92697, USA*
[*]*f.capolino@uci.edu*
http://capolino.eng.uci.edu

Abstract: We investigate local electromagnetic field enhancements in oligomers of plasmonic nanospheres. We first evaluate via full-wave simulations the field between spheres in several oligomer systems: linear dimers, linear trimers, trimers 60°, trimers 90° and linear quadrumers. To gain a better understanding of the field enhancement values, we compare the results with local fields in a hexagonal close-packed (HCP) configuration with same structural dimensions. We then inter-relate the field enhancement values found via full-wave simulations to SERS enhancements of actual fabricated self-assembled oligomers. We find that linear oligomers provide the largest field enhancement values. Finally, we provide closed-form formulas for the prediction of the resonance frequency responsible for field enhancement in linear oligomers, namely dimers, trimers and quadrumers, modeling each nanosphere as a single electric dipole. These formulas provide with resonance values less than 7% shifted when compared to full-wave results even when the gap between spheres is only about one fifth of the radius, showing the powerfulness of dipolar approximations. The results shown in this paper demonstrate that ad hoc clusters of nanospheres can be designed and fabricated to obtain larger field enhancements than with the HCP structure and this may pave the way for the development of improved sensors for molecular spectroscopy.

OCIS codes: (160.3918) Metamaterials; (250.5403) Plasmonics; (240.6695) Surface-enhanced Raman scattering; (050.6624) Subwavelength structures; (220.4241) Nanostructure fabrication.

References and links

1. S. Steshenko, F. Capolino, P. Alitalo, and S. Tretyakov, "Effective model and investigation of the near-field enhancement and subwavelength imaging properties of multilayer arrays of plasmonic nanospheres," Phys. Rev. E Stat. Nonlin. Soft Matter Phys. **84**(1), 016607 (2011).
2. B. P. Rand, P. Peumans, and S. R. Forrest, "Long-range absorption enhancement in organic tandem thin-film solar cells containing silver nanoclusters," J. Appl. Phys. **96**(12), 7519–7526 (2004).
3. A. J. Haes and R. P. V. Duyne, "Preliminary studies and potential applications of localized surface plasmon resonance spectroscopy in medical diagnostics," Expert Rev. Mol. Diagn. **4**(4), 527–537 (2004).
4. K. Hering, D. Cialla, K. Ackermann, T. Dörfer, R. Möller, H. Schneidewind, R. Mattheis, W. Fritzsche, P. Rösch, and J. Popp, "SERS: a versatile tool in chemical and biochemical diagnostics," Anal. Bioanal. Chem. **390**(1), 113–124 (2008).
5. L. Gunnarsson, E. J. Bjerneld, H. Xu, S. Petronis, B. Kasemo, and M. Kall, "Interparticle coupling effects in nanofabricated substrates for surface-enhanced Raman scattering," Appl. Phys. Lett. **78**(6), 802–804 (2001).
6. D. A. Genov, A. K. Sarychev, V. M. Shalaev, and A. Wei, "Resonant Field Enhancements from Metal Nanoparticle Arrays," Nano Lett. **4**(1), 153–158 (2004).
7. E. Hao and G. C. Schatz, "Electromagnetic fields around silver nanoparticles and dimers," J. Chem. Phys. **120**(1), 357–366 (2004).
8. K. Imura, H. Okamoto, M. K. Hossain, and M. Kitajima, "Visualization of localized intense optical fields in single gold-nanoparticle assemblies and ultrasensitive Raman active sites," Nano Lett. **6**(10), 2173–2176 (2006).

#184656 - $15.00 USD Received 1 Feb 2013; revised 7 Mar 2013; accepted 13 Mar 2013; published 26 Mar 2013

9. D. W. Brandl, N. A. Mirin, and P. Nordlander, "Plasmon Modes of Nanosphere Trimers and Quadrumers," J. Phys. Chem. B **110**(25), 12302–12310 (2006).
10. C. E. Talley, J. B. Jackson, C. Oubre, N. K. Grady, C. W. Hollars, S. M. Lane, T. R. Huser, P. Nordlander, and N. J. Halas, "Surface-Enhanced Raman Scattering from Individual Au Nanoparticles and Nanoparticle Dimer Substrates," Nano Lett. **5**(8), 1569–1574 (2005).
11. T. Vo-Dinh, "Surface-enhanced Raman spectroscopy using metallic nanostructures," TRAC-Trend. Anal. Chem. **17**, 557–582 (1998).
12. K. Kneipp, H. Kneipp, and J. Kneipp, "Surface-enhanced Raman scattering in local optical fields of silver and gold nanoaggregates - From single-molecule Raman spectroscopy to ultrasensitive probing in live cells," Acc. Chem. Res. **39**(7), 443–450 (2006).
13. K. Kneipp, H. Kneipp, I. Itzkan, R. R. Dasari, and M. S. Feld, "Surface-enhanced Raman scattering and biophysics," J. Phys.- Condes. Matter **14**(18), R597–R624 (2002).
14. J. Mock, S. Norton, S. Y. Chen, A. Lazarides, and D. Smith, "Electromagnetic Enhancement Effect Caused by Aggregation on SERS-Active Gold Nanoparticles," Plasmonics **6**(1), 113–124 (2011).
15. O. Rabin and S. Y. Lee, "SERS Substrates by the Assembly of Silver Nanocubes: High-Throughput and Enhancement Reliability Considerations," J. Nanotechnol. **2012**, 870378 (2012).
16. A. J. Pasquale, B. M. Reinhard, and L. Dal Negro, "Engineering Photonic-Plasmonic Coupling in Metal Nanoparticle Necklaces," ACS Nano **5**(8), 6578–6585 (2011).
17. A. M. Schwartzberg, C. D. Grant, A. Wolcott, C. E. Talley, T. R. Huser, R. Bogomolni, and J. Z. Zhang, "Unique gold nanoparticle aggregates as a highly active surface-enhanced Raman scattering substrate," J. Phys. Chem. B **108**(50), 19191–19197 (2004).
18. B. Yan, S. V. Boriskina, and B. M. Reinhard, "Optimizing Gold Nanoparticle Cluster Configurations ($n \leq 7$) for Array Applications," J Phys Chem C Nanomater Interfaces **115**(11), 4578–4583 (2011).
19. B. Yan, A. Thubagere, W. R. Premasiri, L. D. Ziegler, L. Dal Negro, and B. M. Reinhard, "Engineered SERS Substrates with Multiscale Signal Enhancement: Nanoparticle Cluster Arrays," ACS Nano **3**(5), 1190–1202 (2009).
20. G. V. P. Kumar, "Plasmonic nano-architectures for surface enhanced Raman scattering: a review," J. Nanophoton. **6**(1), 064503–064520 (2012).
21. X. Gong, Y. Bao, C. Qiu, and C. Y. Jiang, "Individual nanostructured materials: fabrication and surface-enhanced Raman scattering," Chem. Commun. (Camb.) **48**(56), 7003–7018 (2012).
22. B. Gao, Y. Alvi, D. Rosen, M. Lav, and A. R. Tao, "Designer nanojunctions: orienting shaped nanoparticles within polymer thin-film nanocomposites," Chem. Commun. (Camb.) (2013), doi:10.1039/c2cc37158h.
23. S. M. Adams, S. Campione, J. D. Caldwell, F. J. Bezares, J. C. Culbertson, F. Capolino, and R. Ragan, "Non-lithographic SERS Substrates: Tailoring Surface Chemistry for Au Nanoparticle Cluster Assembly," Small **8**(14), 2239–2249 (2012).
24. L. Brown, T. Koerner, J. H. Horton, and R. D. Oleschuk, "Fabrication and characterization of poly(methylmethacrylate) microfluidic devices bonded using surface modifications and solvents," Lab Chip **6**(1), 66–73 (2006).
25. J. H. Choi, S. M. Adams, and R. Ragan, "Design of a versatile chemical assembly method for patterning colloidal nanoparticles," Nanotechnology **20**(6), 065301 (2009).
26. T. Xu, H.-C. Kim, J. DeRouchey, C. Seney, C. Levesque, P. Martin, C. M. Stafford, and T. P. Russell, "The influence of molecular weight on nanoporous polymer films," Polymer (Guildf.) **42**(21), 9091–9095 (2001).
27. R. A. Segalman, A. Hexemer, and E. J. Kramer, "Effects of Lateral Confinement on Order in Spherical Domain Block Copolymer Thin Films," Macromolecules **36**(18), 6831–6839 (2003).
28. E. W. Edwards, M. F. Montague, H. H. Solak, C. J. Hawker, and P. F. Nealey, "Precise Control over Molecular Dimensions of Block-Copolymer Domains Using the Interfacial Energy of Chemically Nanopatterned Substrates," Adv. Mater. **16**(15), 1315–1319 (2004).
29. P. B. Johnson and R. W. Christy, "Optical Constants of the Noble Metals," Phys. Rev. B **6**(12), 4370–4379 (1972).
30. L. A. Sweatlock, S. A. Maier, H. A. Atwater, J. J. Penninkhof, and A. Polman, "Highly confined electromagnetic fields in arrays of strongly coupled Ag nanoparticles," Phys. Rev. B **71**(23), 235408 (2005).
31. S. Zou, N. Janel, and G. C. Schatz, "Silver nanoparticle array structures that produce remarkably narrow plasmon lineshapes," J. Chem. Phys. **120**(23), 10871–10875 (2004).
32. V. Myroshnychenko, J. Rodríguez-Fernández, I. Pastoriza-Santos, A. M. Funston, C. Novo, P. Mulvaney, L. M. Liz-Marzán, and F. J. García de Abajo, "Modelling the optical response of gold nanoparticles," Chem. Soc. Rev. **37**(9), 1792–1805 (2008).
33. S. M. Adams, S. Campione, F. Capolino, and R. Ragan, "Directing cluster formation of Au nanoparticles from colloidal solution," Langmuir dx.doi.org/10.1021/la3051719 (2013).
34. K. H. Su, Q. H. Wei, X. Zhang, J. J. Mock, D. R. Smith, and S. Schultz, "Interparticle Coupling Effects on Plasmon Resonances of Nanogold Particles," Nano Lett. **3**(8), 1087–1090 (2003).
35. K. L. Wustholz, A.-I. Henry, J. M. McMahon, R. G. Freeman, N. Valley, M. E. Piotti, M. J. Natan, G. C. Schatz, and R. P. Van Duyne, "Structure-Activity Relationships in Gold Nanoparticle Dimers and Trimers for Surface-Enhanced Raman Spectroscopy," J. Am. Chem. Soc. **132**(31), 10903–10910 (2010).
36. C. F. Bohren and D. R. Huffman, *Absorption and Scattering of Light by Small Particles* (Wiley, 1983).

#184656 - $15.00 USD Received 1 Feb 2013; revised 7 Mar 2013; accepted 13 Mar 2013; published 26 Mar 2013

37. S. Steshenko and F. Capolino, "Single Dipole Approximation for Modeling Collections of Nanoscatterers," in *Theory and Phenomena of Metamaterials*, F. Capolino, ed. (CRC Press, 2009, Chap. 8).
38. J. D. Jackson, *Classical Electrodynamics* (Wiley, 1998).
39. N. K. Grady, N. J. Halas, and P. Nordlander, "Influence of dielectric function properties on the optical response of plasmon resonant metallic nanoparticles," Chem. Phys. Lett. **399**(1-3), 167–171 (2004).
40. S. Campione, S. Steshenko, M. Albani, and F. Capolino, "Complex modes and effective refractive index in 3D periodic arrays of plasmonic nanospheres," Opt. Express **19**(27), 26027–26043 (2011).
41. M. A. Vincenti, S. Campione, D. de Ceglia, F. Capolino, and M. Scalora, "Gain-assisted harmonic generation in near-zero permittivity metamaterials made of plasmonic nanoshells," New J. Phys. **14**(10), 103016 (2012).
42. A. Vallecchi, S. Campione, and F. Capolino, "Symmetric and antisymmetric resonances in a pair of metal-dielectric nanoshells: tunability and closed-form formulas," J. Nanophoton. **4**(1), 041577 (2010).

1. Introduction

Metal nanoarchitectures, such as arrangements of nanosphere clusters with nm (<10 nm) separation, have application in many technologies, including medical diagnostics, solar cells, and sensors, because of the strong near-field plasmonic coupling and local field enhancement that arise between nanospheres in such configurations [1–3]. Moreover, metal nanoarchitectures may lead to strong surface enhanced Raman scattering (SERS) intensities [4] depending on parameters such as size, shape, morphology, arrangement, and local environment.

SERS intensities of the adsorbates rhodamine 6G and thiophenol from substrates consisting of arrays of electromagnetically coupled silver nanoparticles on silicon [hexagonal close-packed (HCP) configuration] were found to increase rapidly with decreasing inter-particle separation in [5], signaling the importance of strong inter-particle coupling effects in SERS. Similar conclusions were reported in [6]. The discrete dipole approximation has been employed to investigate the electromagnetic fields in monomers and dimers of silver nanoparticles with emphasis on what size, shape, and arrangement leads to the largest local electric field enhancement near the particle surfaces [7]. For the dimers case, the authors of [7] have shown that the spacing of the particles in the dimer plays a crucial role in the field enhancement. In [8], the electric field has been shown to be confined at an interstitial site in the aggregate (dimers or trimers of gold nanospheres). Plasmon energies and absorption spectra of triangular trimers and square quadrumers have been analyzed in [9] using group theory. The possibility of achieving large field enhancements has also been shown in [9]. SERS intensities for individual Au nanospheres, nanoshells, and nanosphere and nanoshell dimers coated with non-resonant molecules were measured in [10], showing also that suitably fabricated nanoshells can provide SERS enhancements comparable to nanosphere dimers.

An overview of the development and application in chemical, environmental and biomedical areas of SERS techniques using metal-coated nanostructures on solid substrates has been shown in [11]. Extremely high SERS enhancement levels can occur for molecules attached to silver and gold nanoclusters making them very promising tools for studies of small structures in biological materials, such as cellular compartments [12, 13]. An experimental study of SERS enhancement from molecules adsorbed on the surface of individual clusters of gold nanoparticles of two types, namely, nanospheres and nanocylinders, has been performed in [14], where the authors have also compared the signal from clusters of two, three, four, and five nanoparticles with the signal from single particles. They have shown that the scaling of SERS intensities from clusters of nanospheres is non-linear with the number of particles, in contrast to the linear dependence in the case of nanocylinders. The non-linear scaling was found to be consistent with the near-field enhancement from inter-particle coupling simulated for clusters of spheres arranged in representative observed geometries. The variations in SERS enhancement factors from clusters of nanocubes were analyzed in [15], and correlated with cluster size and configuration, as well as laser frequency and polarization, showing an increase in the reproducibility of the enhancement and an increase in the average enhancement values by increasing the number of nanocubes in the cluster, up to 4 nanocubes per cluster.

#184656 - $15.00 USD Received 1 Feb 2013; revised 7 Mar 2013; accepted 13 Mar 2013; published 26 Mar 2013

Light-scattering and field localization properties of circular loops of closely spaced gold nanoparticles have been shown in [16], aiming at optimizing their near-field properties for plasmon-enhanced spectroscopy and sensing. Gold nanoparticle clusters have been shown to be an excellent substrate for SERS applications for several biological molecules in [17]. Nanosphere cluster arrays (made of clusters of up to seven 60 nm gold nanospheres) have been analyzed in [18] as a function of size and cluster geometry through a combination of experimental spectroscopy and Mie theory calculations, pointing out the polarization-insensitive responses and high electric field intensity enhancements of trimers and heptamers configurations. This kind of arrays has been also studied in [19], showing the dependence of SERS intensity on the number of particles per unit cell cluster as well as the cluster edge to edge separation. A review of SERS in metallic nanostructures arising from electromagnetic hot spots has been presented in [20]. An overview on the fabrication and SERS studies of individual nanoparticles, nanojunctions and hierarchical nanoaggregates has been recently reported in [21]. The fabrication of self-assembled nanojunctions and their predisposition to generate field hot spots have recently been discussed in [22].

We have recently shown in [23] that large SERS signal enhancement and good point-to-point reproducibility is achievable using a completely non-lithographic fabrication process, thereby producing SERS substrates having high performance at low cost. We are thus now interested in having a deeper insight of the field enhancement achievable by using representative metal clusters: linear dimers, linear trimers, trimers 60°, trimers 90° and linear quadrumers of nanospheres. In particular, we perform full-wave simulations using a finite element method (FEM) in the frequency domain (using High Frequency Structure Simulator - HFSS - by Ansys Inc.) and a finite-difference time-domain (FDTD) method (using FDTD Solutions by Lumerical Solutions Inc.).

Our work significantly differs from the ones previously described for the following reasons. We aim to analyze the resonance conditions of different clusters for achieving maximum SERS field enhancement, varying geometrical dimensions. In particular, we show that linear oligomers morphologically lead to stronger enhancement values, at the cost of dependence on the polarization of the illuminating wave. We perform SERS measurements in self-assembled fabricated substrates and inter-relate experimental and simulation results. Furthermore, we provide closed-form formulas that allow the prediction of the resonance wavelengths of linear oligomers with an error less than 7% with respect to full-wave results when the gap between nanospheres is even as small as about one fifth of the radius. Finally, we compare enhancements in oligomers to enhancements in HCP configuration with same structural dimensions, providing evidence that the former exhibit larger enhancement values, paving the way for extremely large SERS enhancements, for example. To the authors' knowledge, there has not been a direct proof that ad hoc oligomer designs might provide larger SERS enhancements than ordered HCP configurations with same structural dimensions, and this is an important result that should be taken into account for future designs.

2. Field enhancement in clusters of plasmonic nanospheres

The fabrication procedure of a self-assembled SERS substrate is schematically illustrated in Fig. 1(a). The process begins with functionalizing citrate-stabilized ≈23nm Au nanospheres with thioctic acid ligands in colloidal solution for subsequent assembly on a chemically patterned substrate. The substrates have a thin film of polystyrene-block-poly(methyl methacrylate), PS-b-PMMA, on its surface where PMMA regions are functionalized with primary amine groups using ethylenediamine/dimethylsulfoxide (ED/DMSO) solution [24]. 1-Ethyl-3-[3-dimethylaminopropyl] carbodiimidehydrochloride (EDC), via coordination cross-linking chemistry with N-hydroxysulfosuccinimide (S-NHS), was then used to anchor the Au nanospheres onto functionalized PMMA domains [25]. A scanning electron microscopy (SEM) image of a fabricated sample is shown in Fig. 1(b). Single Au

#184656 - $15.00 USD Received 1 Feb 2013; revised 7 Mar 2013; accepted 13 Mar 2013; published 26 Mar 2013

nanospheres, dimers, trimers, and quadrumers are observed on the sample surface, in addition to more complicated clusters. SERS measurements of benzenethiol molecules on similarly fabricated substrates with a high areal coverage of nanosphere oligomers were previously shown to lead to low molecular detection limits [23].

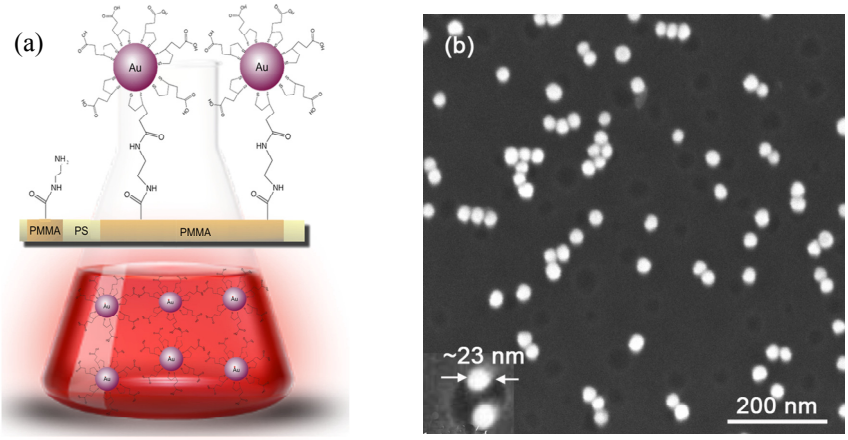

Fig. 1. (a) Schematic of self-assembly fabrication procedure (beaker drawing) where colloidal Au nanospheres are chemically functionalized in solution to produce Au nanosphere oligomers on chemically patterned diblock copolymer surfaces for use as SERS substrates. (b) SEM image showing the types of Au oligomers observed on a fabricated surface. The inset shows a close-up view of a dimer, where the Au nanosphere diameter is approximately 23 nm.

We then perform full-wave simulations of selected fabricated clusters of nanospheres with the aim of demonstrating the formation of field hot spots in experimentally achievable systems. In previous work, we have found Au nanoparticle oligomers are influenced by the shape of the chemical domain [25]. Thus integrating the chemical assembly process referred to here with ordered diblock copolymer surfaces [26–28] is a promising approach for selecting between triangular type oligomers and linear oligomers. The simulated system is reported in the left side of Fig. 2 and is composed of Au nanospheres having diameter of 23 nm, in agreement with performed dynamic light scattering measurements of nanosphere diameters (with Au permittivity matching the values from [29]). [Dynamic light scattering, also known as photon correlation spectroscopy, is a technique that enables the measurement of the size of particles in solution by correlating their relative Brownian motion using the Stokes Einstein relation.] The nanospheres have been assumed to be embedded in a layer with dielectric constant of 2.47 (40 nm thickness) which accounts for the PMMA layer thickness and includes a homogeneous layer of benzenethiol molecules on top, on top of a silicon substrate (same setup of [23]). The gap between the nanospheres is assumed to be 2 nm for the simulations in this section as typically observed in SEM images of our fabricated SERS substrates that rely on Brownian motion (i.e., diffusive movement of the nanospheres in colloidal solution) to bring Au nanospheres to PMMA regions. The same inter-particle distance was used in HCP structures for accurate comparison. For simplicity of calculations, we assume that the clusters in Fig. 2 are arrayed in a square lattice, with a period large enough so that arrays unit cells are weakly coupled to insignificantly affect the maximum field between the nanospheres in a cluster. We then show in Fig. 2(a)-2(i) normalized electric field magnitude maps (with respect to their relative maximum) showing the magnitude (of the phasor) of the electric field outside of the nanospheres retrieved from a FEM-based full-wave simulation for x and y polarizations of the illumination. The field maps depict a region of space in the x-y plane at the location indicated by the dashed red line in the simulation setup reported in Fig. 2; the polarization of the incident wave is also sketched by an arrow in each part Fig. 2(a)-2(i). The insets in Fig. 2(a)-2(e) are SEM images of oligomers observed in

#184656 - $15.00 USD Received 1 Feb 2013; revised 7 Mar 2013; accepted 13 Mar 2013; published 26 Mar 2013

experiments. The results in Fig. 2(a)-2(i) demonstrate the rise of field hot spots between nanospheres.

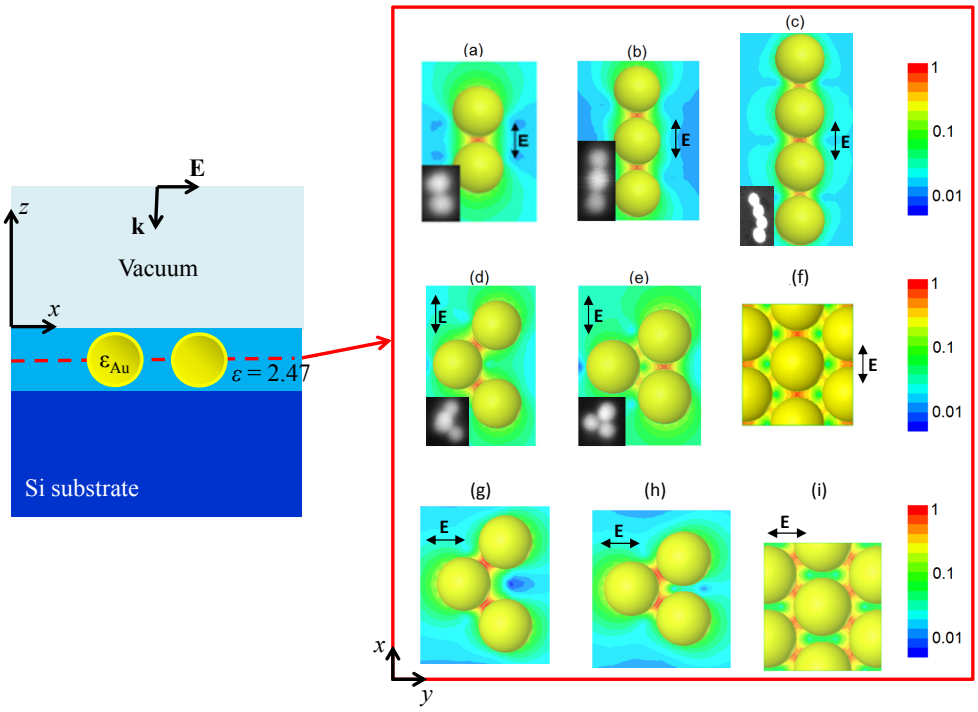

Fig. 2. Schematic of the optical setup employed in simulations. Normalized electric field magnitude maps (outside of the nanospheres) evaluated at the plane indicated by the red dashed line for various clusters and for the HCP configuration under (a-f) *x* polarized and (g-i) *y* polarized illumination at 633 nm, typical laser wavelength. Note the field hot spots between the nanospheres. Numerical results are obtained via FEM. SEM images of self-assembled oligomers are shown as insets in (a-e).

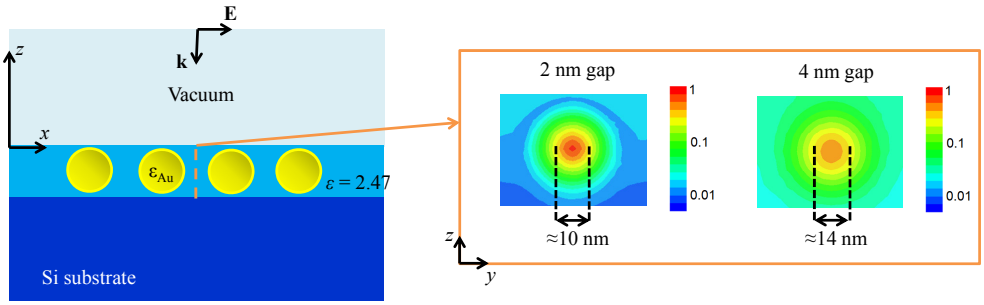

Fig. 3. Normalized electric field magnitude maps on the plane indicated by the orange dashed line at the midpoint of a quadrumer at 633 nm with gap between nanospheres of 2 nm and 4 nm, showing the field confinement.

To better understand the field localization properties, we plot in Fig. 3 the normalized electric field magnitude map on the plane indicated by the orange dashed line at the midpoint of a quadrumer at 633 nm. In particular, we observe that the field diminishes by 10 dB (i.e., 3.16 times) at a distance of about 5 nm from the center when considering 2 nm gaps, and at a distance of about 7 nm from the center when considering 4 nm gaps (in agreement with the results reported in [30] for silver nanoparticles, where the reader is addressed for a deeper

#184656 - $15.00 USD Received 1 Feb 2013; revised 7 Mar 2013; accepted 13 Mar 2013; published 26 Mar 2013

analysis onto field confinement versus gap size). One may then ask whether for practical applications it is better to have more localized, strong fields rather than lower fields more spread in space. We postpone this analysis to a future effort as we move onto justifying experimental results on our fabricated samples.

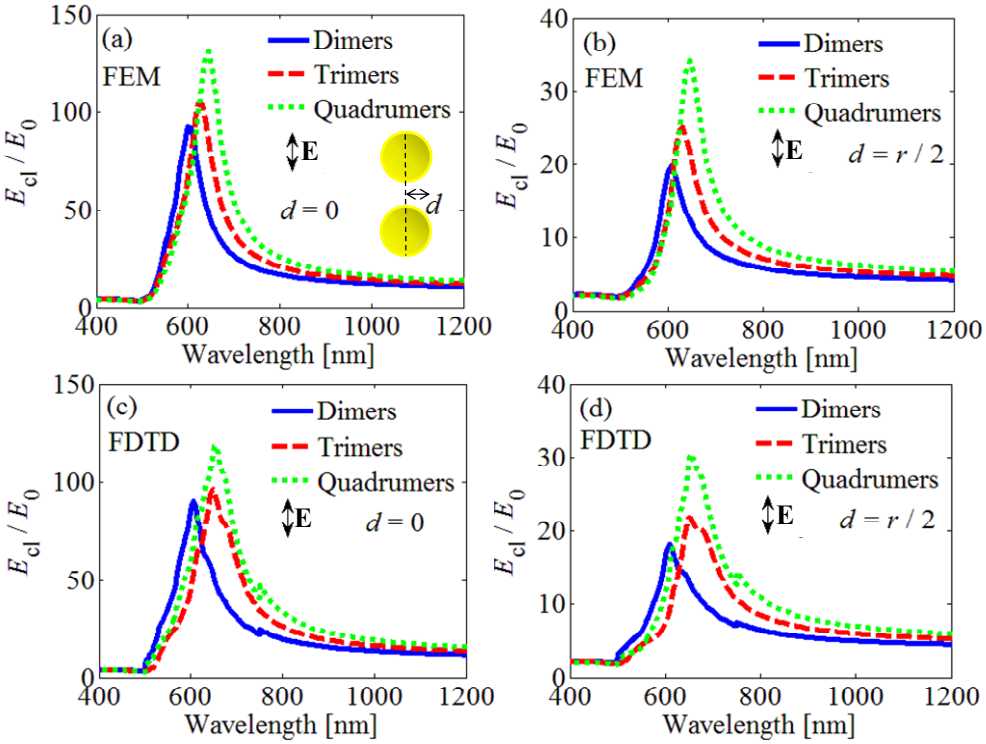

Fig. 4. Field enhancement E_{cl} / E_0 versus illumination wavelength for x polarized illumination for linear oligomers (assuming particles with 23 nm diameter and 2 nm gap) retrieved via FEM and FDTD full-wave simulations, in good agreement. Note the large field enhancement when the oligomers are resonating around 620 nm. Note also the different scales in (a)-(d) for clarity of presentation of the results.

After having understood the large localization of fields in Fig. 2-3, we are interested in the strength of the field that can be achieved in different oligomer configurations. Thus the cluster field enhancement, intended as E_{cl} / E_0, occurring between the nanospheres is calculated, where E_0 is the field magnitude without clusters (still accounting for the multilayered environment in simulation) and E_{cl} is the field magnitude with clusters. We illuminate again each structure with a plane wave orthogonal to the surface, x [as in Fig. 2(a)-2(f)] and y [as in Fig. 2(g)-2(i)] polarized for the range of excitation wavelengths between 400 and 1200 nm. The field enhancement results were evaluated exactly at equal distance between the nanospheres, where the field is stronger in Fig. 2(a)-2(i) and are summarized in Figs. 4, 5, 6 for x and y polarizations at two different locations, namely $d = 0$ and $d = r / 2$, i.e., at and close to the symmetry longitudinal axis. For example, for the linear quadrumer case, the field enhancement has been evaluated between the inner spheres. The parameter d represents the distance in the direction orthogonal to the gap axis. For clarity, the meaning of d is schematically shown in the inset in Fig. 4(a) for a dimer configuration. For x polarization, the result pertaining to the linear oligomers (Fig. 4) is also reproduced via a FDTD-based full-wave simulation, which is in good agreement with the FEM result. In particular, the field enhancement retrieved via FDTD is slightly smaller than the FEM one, whereas the resonance wavelengths predicted by the two full-wave simulations are in good agreement. The

#184656 - $15.00 USD Received 1 Feb 2013; revised 7 Mar 2013; accepted 13 Mar 2013; published 26 Mar 2013

agreement between the two very different full-wave simulators attests the reliability of the data shown in this paper.

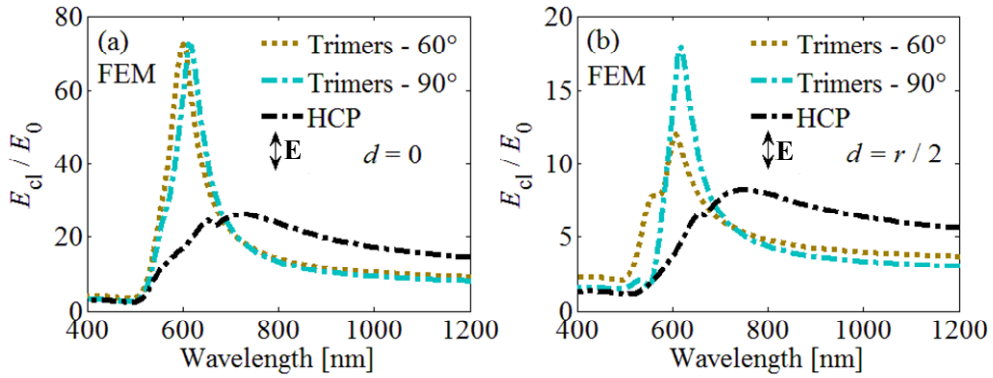

Fig. 5. As in Fig. 4, field enhancement for trimers 60° and 90°, and HCP retrieved via FEM full-wave simulation. Note the large field enhancement when the oligomers are resonating around 600 nm. Note also the different scales in (a)-(b) for clarity of presentation of the results.

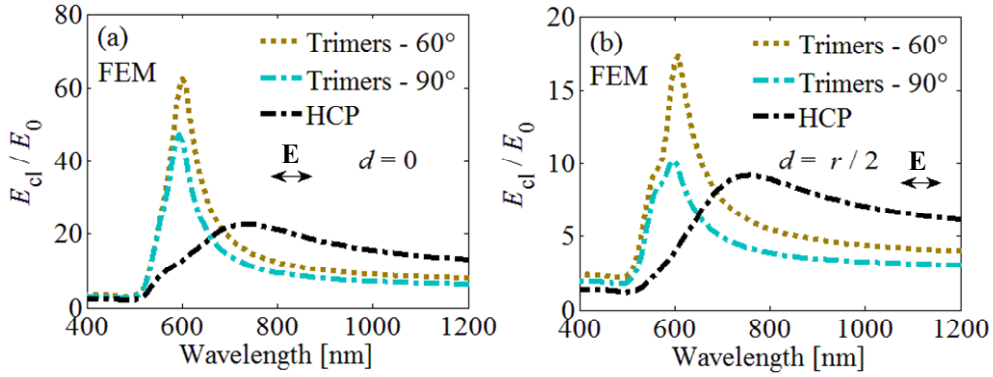

Fig. 6. As in Fig. 5, for *y* polarized illumination. Note the large field enhancement when the oligomers are resonating around 600 nm. Note also the different scales in (a)-(b) for clarity of presentation of the results.

The data in Figs. 4-6 leads to many observations as detailed in the following. Stronger field enhancement (with peak of about 2 orders of magnitude) is achieved with linear oligomers (dimers, trimers, quadrumers) around the band 500-800 nm with respect to a HCP configuration and also to other trimer configurations. Remarkably, the HCP with the same structural dimensions resonates at about 730 nm and it is peculiar that it does not allow for field enhancements stronger than about 26. The linear trimer resonance frequency is red shifted with respect to the dimer's one, also providing a larger field enhancement, as it happens also in the linear quadrumer case with respect to the linear trimer one. This result is in agreement with what reported in [31], where one can also infer that increasing number of particles in a linear oligomer system (even larger than 4, the maximum analyzed here) may provide with larger enhancements at red shifted frequency values, till saturation is reached (i.e., resemblance to an infinite chain of nanospheres). Note also that the field enhancement has a nonlinear dependence on the number of spheres. For example, resonance saturation has been estimated to be reached with 20 particles for Ag particles in free space in [30]. Similar arguments may apply also to the field enhancement. When considering triangular trimers and HCP, one polarization, *x*, leads to slightly stronger field enhancement with respect to the other, *y*. In particular, linear oligomers provide stronger field enhancement than triangular clusters, when the polarization matches with the axis of the linear cluster. Vice versa,

#184656 - $15.00 USD Received 1 Feb 2013; revised 7 Mar 2013; accepted 13 Mar 2013; published 26 Mar 2013

triangular clusters provide slightly weaker field enhancement than linear oligomers, still considerably larger than HCP, but their field enhancement is robust with respect to the polarization of the incident wave. The results regarding resonance wavelengths and maximum field enhancements reported in Figs. 4-6 are summarized in Table 1 for better readability. These results show that ad hoc clusters can be designed and fabricated to obtain larger field enhancements than with the HCP structure for the particle dimensions considered in this paper. Therefore, they show that the increased number of oligomer arrangements is important for use in sensing applications and molecular spectroscopy.

Table 1. Summary of the resonance wavelengths (in nm) and maximum field enhancements E_{cl} / E_0 for the oligomers and the HCP structure simulated via FEM in Figs. 4-6.

Configuration	Resonance wavelength (nm)	Field enhancement
Dimer	606	92
Linear trimer	625	105
Linear quadrumer	645	131
Trimer 60°	600 (*x*-pol) ; 600 (*y*-pol)	72.4 (*x*-pol) ; 62.3 (*y*-pol)
Trimer 90°	612 (*x*-pol) ; 594 (*y*-pol)	72.5 (*x*-pol) ; 47.2 (*y*-pol)
HCP	723 (*x*-pol) ; 732 (*y*-pol)	26.1 (*x*-pol) ; 22.6 (*y*-pol)

3. Strong field enhancement for surface enhanced Raman scattering (SERS)

The promising results relative to substrates with discrete clusters of nanospheres versus substrates with higher uniformity and coverage (i.e., HCP) reported in the previous section shed light onto the full benefits of the former, and thus motivate further analysis. Chemical assembly as described in Fig. 1 produces closely spaced nanospheres in discrete clusters. While using self-assembly methods there is a distribution of different types of clusters observed on the surface; we then analyze SERS experimental data from substrates of such surfaces with Au nanospheres arranged in clusters with adsorbed benzenethiol molecules on top. The measured SERS intensity of benzenethiol vibrational modes is shown in Fig. 7(a) (where the υ mode corresponding to a Raman shift of 1571 cm^{-1} is explicitely indicated). The blue dashed line corresponds to a sample that has 16% of Au oligomers on the surface (magnified 20 times). The red solid line has instead 90% of Au oligomers. The remaining 84% and 10%, respectively, consists of isolated nanospheres. There is a clear increase in SERS intensity when the sample surface is composed primarily of oligomers despite the fact there is a distribution of different types of oligomers on the surface. Representative oligomers are shown as insets in Fig. 2(a)-2(e). The SERS enhancement values from experimental data have been retrieved as explained in the Supplementary Information in [23], obtaining 2×10^8 from the sample with 16% coverage and 3×10^9 from the sample with 90% coverage, when illuminating with a laser at 633 nm. The reason of this large SERS enhancement is mainly attributed to the highly strong and localized field enhancement observed in Sec. 2. It is well known that the SERS enhancement is proportional to the fourth power of the field enhancement, therefore we report in Fig. 7(b) the theoretical SERS enhancement calculated as $(E_{cl} / E_0)^4$ using the result computed via the FEM-based full-wave simulation in Fig. 4 pertaining to the linear oligomer configurations. Linear oligomers provide with the largest enhancements among all the configurations shown in Figs. 4-6. With quadrumers, we estimate SERS enhancements as high as 3×10^8, purely looking at the field. This enhancement is however smaller than the maximum value of 3×10^9 shown in the experimental data pertaining to the sample with 90% coverage of Fig. 7(a). This difference is expected for three reasons. First, other more complex oligomer configurations observed in SEM images than the representative ones analyzed in this paper are present and may induce a stronger field enhancement. Second, in the calculations we have completely neglected any molecule-cluster near-field interaction, which might further enhance scattering. Accurate investigations accounting for such interactions will be carried out in the future, for example

#184656 - $15.00 USD Received 1 Feb 2013; revised 7 Mar 2013; accepted 13 Mar 2013; published 26 Mar 2013

simulations that include dipolar scatterers in the gap between nanospheres to justify higher enhancements than those in Fig. 7(b). Third, we have assumed to have oligomer configurations with 2 nm gaps. However, gap size plays a major role into field enhancement, as shown in the analysis in the next section. Differences in gaps with actual fabricated structures may justify the discrepancies between experimental SERS enhancement and theoretical estimations in Fig. 7.

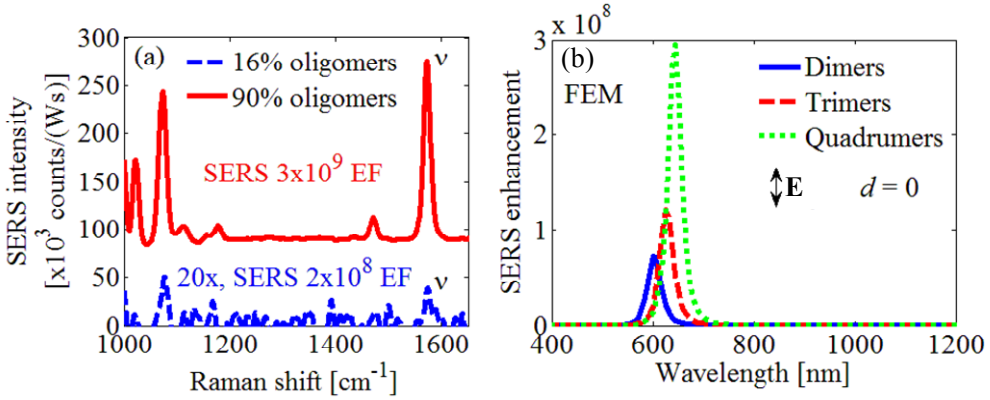

Fig. 7. (a) SERS experimental data from substrates of Au nanospheres with adsorbed benzenethiol molecules on top. EF = enhancement factor. (b) Theoretical SERS enhancement [computed as $(E_{cl} / E_0)^4$, i.e., the fourth power of the field enhancements in Sec. 2] for the linear oligomers in Fig. 4.

4. Effect of gap size onto field enhancement

It is expected that stronger field enhancement values are obtained when the nanospheres are very close to each other, i.e., the gap is small, trend shown for example in the case of a dimer in [32]. Electrophoresis deposition (EPD) allows for spacing between nanospheres as low as ≈1 nm [33]. The fabrication method is similar to that described in Sec. 2, with the difference being the EPD method uses the PS-b-PMMA thin film deposited on highly doped Si as the working electrode to drive Au nanospheres to the surface. A Pt electrode is suspended in the aqueous Au nanoparticle solution as the counter electrode. Zeta potential measurements of the thioctic acid functionalized Au nanospheres exhibit a negative zeta potential and thus in solution the nanospheres will be attracted to the Si sample surface with the PS-b-PMMA thin film when positive bias is applied. An SEM image of a fabricated substrate using EPD is reported in Fig. 8(a). By comparing the SEM image in Fig. 8(a) with the SEM image in Fig. 1(b), we observe narrower gaps when using EPD. This fact motivates the theoretical analysis shown in what follows. In particular, we are now interested in understanding how the gap size affects the results in Sec. 2 for the linear oligomers, shown to provide the largest enhancements.

The estimated theoretical SERS enhancement for varying gap size is reported in Fig. 8(b)-8(d). Note that a slight increase in the gap size dramatically affects the SERS enhancement, going from about $\approx 10^{10}$ for the quadrumer case with 1 nm gap to about $\approx 3 \times 10^8$ when the gap is 2 nm, i.e., about two orders of magnitude decrease. We note also the resonance blue shift for increasing gap size, in agreement with the results shown in [34]. Note that, although we observed for linear oligomers an increase in the field enhancement with increasing number of particles, the gap between them is the most critical parameter for achieving very strong SERS enhancement that would in principle lead to single molecule detection [35].

#184656 - $15.00 USD Received 1 Feb 2013; revised 7 Mar 2013; accepted 13 Mar 2013; published 26 Mar 2013

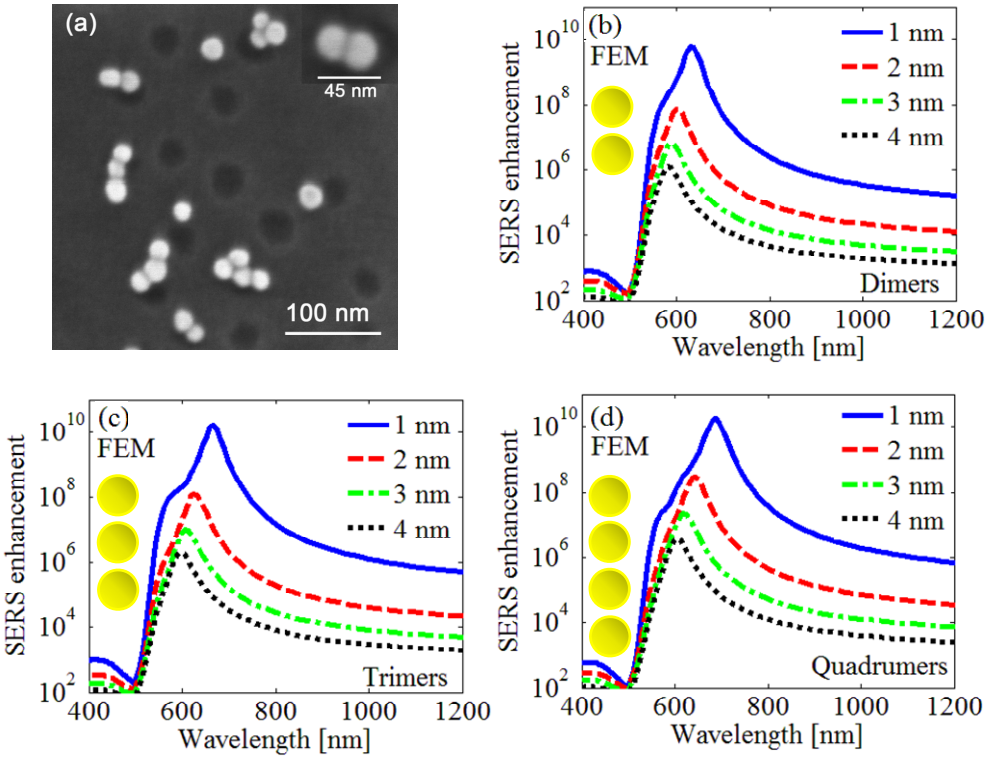

Fig. 8. (a) SEM image showing the types of Au oligomers observed on a fabricated surface using EPD. The inset shows a close-up view of a dimer, where it can be observed that the gap between nanospheres is smaller than the one obtained by fabrication based on Brownian motion in Fig. 1. (b-d) Theoretical SERS enhancement [computed as $(E_{cl} / E_0)^4$, i.e., the fourth power of the field enhancement] for the linear oligomers in Fig. 4 retrieved via FEM full-wave simulations for various gap sizes. Note the decreasing SERS enhancement and the resonance blue shift for increasing gap size.

5. Prediction of resonance frequencies in linear oligomers

As shown in the previous sections, a large field enhancement is observed in the case of oligomers rather than the HCP configuration. Within the oligomers, the linear configurations have provided with the largest enhancements, even though they are limited to a specific polarization of the incident wave. For this reason, in this section we aim at predicting the resonance frequencies of such oligomers providing simple closed-form formulas. These expressions also permit to account for the presence of a host medium with permittivity different from that of free space. We employ the single dipole approximation (SDA) [36, 37] which is a procedure that provides with results with good accuracy when all the dimensions are subwavelength and the gap between nanospheres is approximately the same as the radius (or larger). In the cases analyzed in the previous sections, these conditions are not completely satisfied as the gap is smaller than the nanosphere's radius, thus multipolar contributions may not be negligible. Therefore, the accuracy of the SDA model will be discussed in what follows.

#184656 - $15.00 USD Received 1 Feb 2013; revised 7 Mar 2013; accepted 13 Mar 2013; published 26 Mar 2013

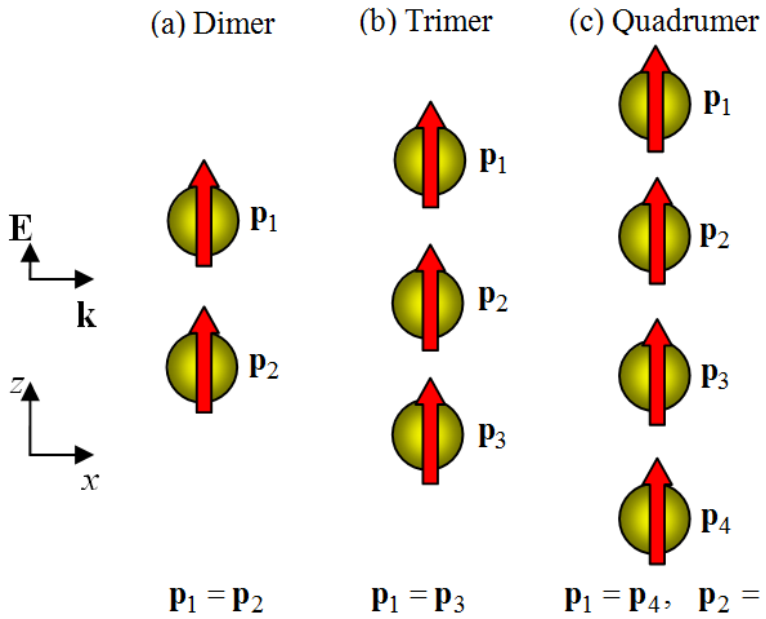

Fig. 9. (a) Dimers, (b) trimers and (c) quadrumers linearly positioned along a direction, for simplicity assumed to be the z direction. The red arrows indicate the distribution of induced dipole moment $\mathbf{p}_i$ for the longitudinal symmetric resonance frequencies.

When a subwavelength metallic nanosphere is immersed in an electric field $\mathbf{E}$, it can be modeled as an electric dipole via SDA [36, 37], for which the induced electric dipole moment is given by $\mathbf{p} = \alpha_{\text{ee}}\mathbf{E}^{\text{loc}}$, where $\mathbf{E}^{\text{loc}}$ is the local electric field at the particle location and α_{ee} is the nanosphere's isotropic electric polarizability. A commonly used expression for the inverse polarizability of a nanosphere is given by the quasi-static approximation including damping correction [37, 38] [electromagnetic fields are assumed to be time harmonic with a $\exp(-i\omega t)$ time variation]

$$\alpha_{\text{ee}}^{-1} = \frac{\varepsilon_m + 2\varepsilon_h}{4\pi\varepsilon_0\varepsilon_h r^3(\varepsilon_m - \varepsilon_h)} - i\frac{k^3}{6\pi\varepsilon_0\varepsilon_h} \tag{1}$$

where ε_h is the relative permittivity of the medium hosting the nanosphere, and ε_0 is the absolute permittivity of free space. Moreover, r is the sphere radius, $k = \omega\sqrt{\varepsilon_h}/c_0 = k_0\sqrt{\varepsilon_h}$ is the host medium wavenumber, with k_0 denoting the free space wavenumber, c_0 the speed of light in free space and ε_m is the relative permittivity of the metallic nanosphere, which is described in this section by the Drude model

$$\varepsilon_m = \varepsilon_\infty - \frac{\omega_p^2}{\omega(\omega + i\gamma)}. \tag{2}$$

In Eq. (2), ε_∞ is a high-frequency fitting parameter, ω_p is the plasma frequency of the metal (expressed in rad/s) and γ is the damping factor (expressed in 1/s). For gold, $\varepsilon_\infty = 9.5$, $\omega_p = 1.36\times10^{16}$ rad/s, and $\gamma = 1.05\times10^{14}$ rad/s [39]. In general, this model provides a reasonably accurate description of the dielectric properties of the metal across the infrared and optical frequency ranges.

#184656 - $15.00 USD Received 1 Feb 2013; revised 7 Mar 2013; accepted 13 Mar 2013; published 26 Mar 2013

In Fig. 9 we report the three linear configurations excited by a normally incident plane wave as in Sec. 2. Such plane wave will excite each nanosphere, which will be polarized along the direction of the electric field **E**; consequently, each nanosphere will have the induced dipole moment $\mathbf{p}_i$, $i = 1, \ldots, 4$, as pictorially depicted by the red arrows in Fig. 9.

The derivation steps of the closed-form formulas for the resonance frequencies of each oligomer system in Fig. 9 are summarized in Appendix A, and the final formulas are here presented and discussed. The resonance frequency for each configuration can be expressed as

$$\omega = \omega_{\text{res}} - i\frac{\gamma}{2}, \qquad \text{with} \qquad \omega_{\text{res}} = \frac{\omega_p}{\sqrt{\varepsilon_t}} K, \tag{3}$$

where $\varepsilon_t = 2\varepsilon_h + \varepsilon_\infty$ and the value of K (under the assumption $\gamma \ll \omega_p$) depends on the oligomer configuration, given in what follows. For the monomer $K = 1$, and for the dimer,

$$K = \sqrt{\frac{1-2q^3}{1-2K_{CM}q^3}}. \tag{4}$$

For the trimer,

$$K = \sqrt{\frac{8-\left(1+3\sqrt{57}\right)q^3}{8-\left(1+3\sqrt{57}\right)K_{CM}q^3}}, \tag{5}$$

and for the quadrumer

$$K = \sqrt{\frac{108-\left(112+\sqrt{69865}\right)q^3}{108-\left(112+\sqrt{69865}\right)K_{CM}q^3}} \tag{6}$$

where

$$K_{CM} = \frac{\varepsilon_\infty - \varepsilon_h}{\varepsilon_\infty + 2\varepsilon_h} \quad \text{and} \quad q = \frac{r}{s}, \tag{7}$$

with s the center-to-center distance between two nanospheres.

Table 2. Resonance wavelengths (in nm) for the linear oligomers in Fig. 9, assuming particles with 23 nm diameter and 2 nm gap.

Method		Resonance wavelength (nm) (relative error)		
		Dimer	Trimer	Quadrumer
(I)	FEM, multilayered environment (Fig. 2)	606	625	645
(II)	FEM, homogeneous environment $\varepsilon_h = 2.47$	600	619	638
(III)	Quasi-static polarizability, using gold Drude model, Eqs. (3)-(6)	558 (7.0%)	578 (6.6%)	592 (7.2%)
(IV)	Mie polarizability and field retardation, using gold Drude model, Eqs. (13)-(15)	569 (5.2%)	593 (4.2%)	610 (4.4%)
(V)	Mie polarizability, field retardation, using experimental gold data [29], Eq. (10)	582 (3.0%)	599 (3.2%)	612 (4.1%)

We summarize in Table 2 the resonance wavelengths for each cluster type (assuming a gap of 2 nm) estimated by using the FEM full-wave results in Fig. 4 using the simulation setup shown in Fig. 2 and referred to as Method (I) in Table 2. We then perform FEM full-wave simulations of an equivalent system in which the clusters are embedded into a

#184656 - $15.00 USD Received 1 Feb 2013; revised 7 Mar 2013; accepted 13 Mar 2013; published 26 Mar 2013

homogeneous space with relative permittivity $\varepsilon_h = 2.47$ [Method (II)]. This result shows that the cluster resonance location is only slightly affected by the presence of the multilayered environment since the spheres are completely inside the layer with permittivity of 2.47. For this reason, we can now use the theoretical model described in Appendix A to oligomers embedded in a homogeneous environment with relative permittivity $\varepsilon_h = 2.47$. First, by using the closed-form formulas in Eqs. (3)-(6), that use the Drude model for gold permittivity, we evaluate the resonance wavelengths summarized in Table 2 [Method (III)] for each cluster type [note that using Eq. (3) the resonance wavelength of an isolated nanosphere is 527 nm]. We note that the simple analytical formulas allow for the prediction of the resonance red shift observed when increasing number of spheres in the linear cluster, and are in fair agreement with full-wave simulations. Note that the theoretical model predicts resonance values blue shifted with respect to the resonances estimated via full-wave simulations. To better express the accuracy of the theoretical model, we calculate the relative error (in %) as

$$Err\% = \frac{\left|\lambda_{\mathrm{FEM}} - \lambda_{\mathrm{th}}\right|}{\lambda_{\mathrm{FEM}}} \times 100 \tag{8}$$

where λ_{FEM} is the resonance wavelength evaluated using the FEM full-wave simulation in homogeneous environment [Method (II)] and λ_{th} the resonance wavelength estimated using the correspondent theoretical model. As mentioned above, multipolar contributions should be included because of the close proximity of the spheres; however, using the closed-form formulas in Eqs. (3)-(6) we observe an error less than about 7% in the estimation of the resonance wavelength even when the gap is about one fifth of the nanosphere's radius, showing that it is sufficient to account for dipolar processes only when estimating the cluster resonance.

Table 3. Resonance wavelengths (in nm) for the linear oligomers in Fig. 9, assuming particles with 23 nm diameter and 4 nm gap.

Method		Resonance wavelength (nm) (relative error)		
		Dimer	Trimer	Quadrumer
(I)	FEM multilayered environment (Fig. 2)	583	594	606
(II)	FEM homogeneous environment $\varepsilon_h = 2.47$	583	594	603
(III)	Quasi-static polarizability, using gold Drude model, Eqs. (3)-(6)	551 (5.5%)	565 (4.9%)	574 (4.8%)
(IV)	Mie polarizability and field retardation, using gold Drude model, Eqs. (13)-(15)	560 (3.9%)	578 (2.7%)	589 (2.3%)
(V)	Mie polarizability, field retardation, using experimental gold data [29], Eq. (10)	576 (1.2%)	586 (1.3%)	596 (1.2%)

For better accuracy of the results, we also model the nanospheres using the Mie electric polarizability [36, 40] in place of the quasi-static expression in Eq. (1), and include field retardation effects [neglected in Eqs. (3)-(6)]. However, this in turn avoids the determination of simple analytical closed-form formulas. Nonetheless, we solve numerically the equations reported in Appendix A and evaluate the resonance wavelengths, also reported in Table 2, Method (IV), in better agreement with FEM results, Method (II), since the relative error *Err* is about 5%, smaller than the one computed when using the closed-form formulas [note that using Method (IV) in this case the resonance wavelength of an isolated nanosphere is 532 nm]. In principle, the estimation of the resonance wavelengths would be even more accurate if a realistic model for the gold permittivity were adopted, as also shown in Table 2, Method (V), with a smaller relative error *Err* of about 4%, when using gold permittivity data from [26].

#184656 - $15.00 USD Received 1 Feb 2013; revised 7 Mar 2013; accepted 13 Mar 2013; published 26 Mar 2013

In order to show that the SDA model gains accuracy when the gap increases, we show in Table 3 similar results to Table 2 pertaining to linear clusters of nanospheres assuming a gap of 4 nm. Note the reduction of the relative error *Err*, direct proof of the improvement in accuracy, reaching errors of the order of 1% [Method (V), Table 3]. We want to stress that even though with the theoretical model shown here for gaps of the order of 2 nm we achieve an error *Err* of about 7%, the simple closed-form formulas in Eqs. (3)-(6) may be used as guidance for the design of cluster resonances for a required application, such as in resonance with a commercial laser line for molecular spectroscopy. We want to point out that the SDA can be used to retrieve spectral features with good accuracy, as also recently shown in [41].

Finally, we investigate the capability of the simpler but approximate SDA model in the estimation of the field enhancement for linear oligomers as in Fig. 4(a). We assume gold nanospheres [29] with 23 nm diameter and 2 nm gap in a homogeneous environment with $\varepsilon_h = 2.47$. We retrieve the nanospheres' dipole moments by using the model in Appendix A; then, we employ the dyadic Green's function to calculate the field enhancement evaluated as $E_{\mathrm{cl}} / E_{\mathrm{PW}}$ shown in Fig. 10, where E_{PW} is the plane wave field magnitude without clusters and E_{cl} is the field magnitude with clusters, occurring between the nanospheres. We observe the same trends noted in Fig. 4(a) also in the SDA results in Fig. 10, although values are not directly comparable to the ones in Fig. 4(a) as we are analyzing spheres in homogeneous environment (i.e., without substrate).

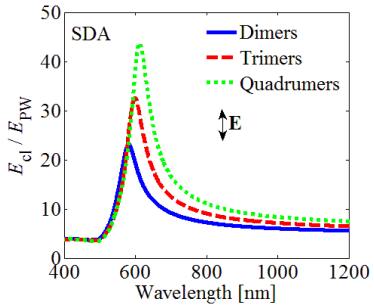

Fig. 10. Field enhancement $E_{\mathrm{cl}} / E_{\mathrm{PW}}$ versus illumination wavelength for *x* polarized illumination for linear oligomers in homogeneous environment (assuming particles with 23 nm diameter and 2 nm gap) retrieved via SDA near-field calculations.

6. Conclusion

We analyze field enhancement in systems of oligomers of plasmonic nanospheres, highly localized between the nanospheres. We observe the generation of large field enhancement values in linear and triangular oligomers when compared to a hexagonally close-packed structure with the same physical dimensions. Within the oligomers, linear systems are found to provide the largest enhancement values. Slightly lower enhancements, but insensitive to the illumination polarization are achieved when using triangular oligomers. We also observe a frequency red shift in the resonances of linear systems when increasing number of spheres. This red shift is estimated by using the provided simple closed-form formulas that allow for the estimation of the resonance wavelengths for each system with about 7% error when the gap is one fifth of the nanosphere's radius. The achieved large field enhancement values provide with the evidence that systems of oligomers may be employed for SERS applications and exhibit the potential to lead to single molecule detection if further improved.

#184656 - $15.00 USD Received 1 Feb 2013; revised 7 Mar 2013; accepted 13 Mar 2013; published 26 Mar 2013

Appendix A: Closed-form formulas for resonances in linear oligomers

Consider the oligomers made of N nanospheres, with $N = 1,\ldots,4$, linearly positioned along a direction, for simplicity assumed to be the z direction in Fig. 9. The local electric field $\mathbf{E}_n^{\mathrm{loc}}$ acting on the n-th particle at $\mathbf{r}_n$ is given by

$$\mathbf{E}_n^{\mathrm{loc}} = \mathbf{E}^{\mathrm{inc}}(\mathbf{r}_n) + \sum_{\substack{m=1 \\ m\neq n}}^{N} \underline{\mathbf{G}}(\mathbf{r}_n, \mathbf{r}_m) \cdot \mathbf{p}_m, \tag{9}$$

where $\underline{\mathbf{G}}(\mathbf{r}_n, \mathbf{r}_m)$ is the dipole dyadic Green's function. Combining Eq. (9) with the information that $\mathbf{p}_n = \alpha_{\mathrm{ee}} \mathbf{E}_n^{\mathrm{loc}}$, we aim at finding the resonance frequencies of the N-spheres system by solving the linear system ($n = 1, \ldots, N$)

$$\sum_{m=1}^{N} \underline{\mathbf{A}}_{nm} \cdot \mathbf{p}_m = \mathbf{E}^{\mathrm{inc}}(\mathbf{r}_n), \quad \underline{\mathbf{A}}_{nm} = \begin{cases} \alpha_{\mathrm{ee}}^{-1} \underline{\mathbf{I}}, & n = m \\ -\underline{\mathbf{G}}(\mathbf{r}_n, \mathbf{r}_m), & n \neq m \end{cases}. \tag{10}$$

Finally, one can retrieve the resonance frequencies by computing the frequency values that are solutions of the homogeneous system in Eq. (10). When a dipole is placed in a homogeneous environment, $\underline{\mathbf{G}}(\mathbf{r}_n, \mathbf{r}_m)$ simply is

$$\underline{\mathbf{G}}(\mathbf{r}_n, \mathbf{r}_m) = \left[c_1 \underline{\mathbf{I}} + c_2 \underline{\boldsymbol{\Psi}}(\mathbf{r}_{nm}) \right], \tag{11}$$

where $\underline{\mathbf{I}}$ is the identity dyad, $\underline{\boldsymbol{\Psi}}(\mathbf{r}_{nm}) = \mathbf{r}_{nm}\mathbf{r}_{nm} / r_{nm}^2$, $\mathbf{r}_n$ and $\mathbf{r}_m$ are the observation and source positions, $\mathbf{r}_{nm} = \mathbf{r}_n - \mathbf{r}_m$ and $r_{nm} = |\mathbf{r}_{nm}|$. Moreover,

$$c_1(r_{nm}) = \frac{e^{ikr_{nm}}}{4\pi\varepsilon_0\varepsilon_h} \left(\frac{k^2}{r_{nm}} + \frac{ik}{r_{nm}^2} - \frac{1}{r_{nm}^3} \right), \quad c_2(r_{nm}) = -\frac{e^{ikr_{nm}}}{4\pi\varepsilon_0\varepsilon_h} \left(\frac{k^2}{r_{nm}} + \frac{3ik}{r_{nm}^2} - \frac{3}{r_{nm}^3} \right). \tag{12}$$

Note that in a homogeneous space $\underline{\mathbf{G}}(\mathbf{r}_n, \mathbf{r}_m) = \underline{\mathbf{G}}(\mathbf{r}_m, \mathbf{r}_n)$ because $\underline{\boldsymbol{\Psi}}(\mathbf{r}) = \underline{\boldsymbol{\Psi}}(-\mathbf{r})$. Also, when the particles are placed along the z direction, $\underline{\boldsymbol{\Psi}}(\mathbf{r}) = \hat{\mathbf{z}}\hat{\mathbf{z}}$.

The resonances for the longitudinal symmetric polarizations (i.e., dipole moments are all in the same direction) are found by solving numerically the following equations, depending on the oligomer configuration. For the monomer, $\alpha_{\mathrm{ee}}^{-1} = 0$ (defining the first Frolich resonance of the isolated nanosphere [36]) whereas for the dimer

$$\alpha_{\mathrm{ee}}^{-1} - c_{12} = 0. \tag{13}$$

For the trimer

$$\alpha_{\mathrm{ee}}^{-2} - c_{13}\alpha_{\mathrm{ee}}^{-1} - 2c_{12}^2 = 0, \tag{14}$$

and for the quadrumer

$$\alpha_{\mathrm{ee}}^{-2} - (c_{12} + c_{14})\alpha_{\mathrm{ee}}^{-1} + c_{12}c_{14} - (c_{12} + c_{13})^2 = 0, \tag{15}$$

where $c_{nm} = c_1(r_{nm}) + c_2(r_{nm})$. When searching for the roots of the polynomials in Eqs. (14) and (15), the roots with the "+" sign should be chosen to select the dipole moments to be all in the same direction.

#184656 - $15.00 USD Received 1 Feb 2013; revised 7 Mar 2013; accepted 13 Mar 2013; published 26 Mar 2013

The equation for a dimer [Eq. (13)] has also been reported in [42]. Here we are interested in deriving the analytical, closed-form expressions for the resonances associated also to trimer and quadrumer linear oligomer systems.

If the particles are small compared to the free space wavelength, it is possible to replace some electrodynamic terms by electrostatic ones. In SDA calculations, this is equivalent to setting $k = 0$ in Eqs. (1) and (12), obtaining

$$\alpha_{\mathrm{ee}}^{-1} = \frac{\varepsilon_m + 2\varepsilon_h}{4\pi\varepsilon_0\varepsilon_h r^3\left(\varepsilon_m - \varepsilon_h\right)}, \quad c_1\left(r_{nm}\right) = -\frac{1}{4\pi\varepsilon_0\varepsilon_h r_{nm}^3}, \quad c_2\left(r_{nm}\right) = \frac{3}{4\pi\varepsilon_0\varepsilon_h r_{nm}^3} \tag{16}$$

but keeping the correct frequency dependent dielectric constant ε_m in Eq. (2). Therefore, after neglecting the dynamic terms [in other words we keep only the $1/r_{nm}^3$ terms in Eq. (12) as in Eq. (16)] and by taking into account that $\gamma \ll \omega_p$, Eq. (10), and consequently the educed expressions in Eqs. (13)-(15), are solved analytically for the resonant angular frequencies leading to the expressions in Eqs. (3)-(6) for longitudinal (i.e., along the linear oligomer axis) electric polarization in Sec. 5.

Acknowledgments

This material is based upon work supported by the National Science Foundation under Grant No. CMMI-1101074 and CHE-0748912. The authors thank Ansys Inc. for providing HFSS that was instrumental in this work. The authors also acknowledge the use of the facilities within the Laboratory for Electron and X-ray Instrumentation (LEXI) at the University of California, Irvine.

#184656 - $15.00 USD Received 1 Feb 2013; revised 7 Mar 2013; accepted 13 Mar 2013; published 26 Mar 2013